"ELEPHANT HIDE" TEXTURE ON THE MOON: PRELIMINARY RESULTS ON TOPOGRAPHIC PROPERTIES. *N. V. Bondarenko[1], M. A. Kreslavsky*[1], *A. Zubarev*[2], *I. Nadezhdina*[2], [1]Earth and Planetary Sciences, University of California – Santa Cruz, Santa Cruz, CA, 95064, USA, mkreslav@ucsc.edu, [2]Moscow State University of Geodesy and Cartography (MIIGAiK), 4 Gorokhovsky by-str., 105064 Moscow, Russia.

Introduction: On the Moon, regolith-covered slopes have a specific subtle meters-to-decameters-scale texture dubbed "elephant hide" texture (EHT) [e.g., 1] or "leathery" [2] texture, or "creeps" [3]. EHT is ubiquitous [3], it occurs on virtually all slopes steeper than ~5° – 8°, regardless of latitude and the slope orientation [4]. EHT appearance and an apparent anisotropy change with the change of the illumination direction; it is difficult to understand EHT relief using images. The formation mechanism of EHT is essentially unknown. Regolith gardening due to micrometeoritic impacts operates like a topographic diffusion [5,6], it smooths down and eventually eliminate any small-scale topography and cannot generate any small-scale rough pattern. The existence of EHT, therefore, requires that some currently unknown mechanism roughens all inclined regolith surfaces surpassing the smoothing action of the micrometeoritic gardening. We analyze EHT topography and occurrence to get clues on that mechanism; here we report preliminary results.

Occurrence: In [4] global distribution of the EHT was analyzed using randomized samples of the surface and global topographic data sets. Because of inevitable misregistration of images with respect to topography that study could not measure the onset slope of EHT formation accurately. Here we used high-resolution DTMs obtained by stereo processing of LROC NAC images [7] for 3 different highland areas. We used low-sun images to detect the presence of EHT, however, for the mapping base we used moderately high-sun orthorectified images that had been utilized for photogrammetric DTM generation. In this way we obtained maps of areas with and without EHT accurately coregistered with topography. Since the longest-wavelength component of EHT topography complicates the DTMs, the background slopes cannot be defined perfectly objectively. We smoothed the DTMs with the median filter with a circular sliding window ~300 m in diameter and took slopes of the smoothed topography as a proxy for the background slopes. **Fig. 1** shows proportions of EHT-bearing and EHT-free area as a function of background slopes for one of the DTMs ("NAC_DTM_SLIPHER1" from the PDS; 48.4°N 160.6°E); for the other two studied sites the results look similar. We see that <u>there is no sharp slope onset of EHT formation</u>; the transition from EHT-free to EHT-bearing terrain is gradual and spans a wide range of slopes. This transition is smeared by observational factors: the inherent uncertainties in determination of the gentle regional slopes and in identification of subtle EHT, however, the visual analysis confirms both presence and absence of EHT at ~3° steep slopes. It is also seen that on very gentle slopes EHT is always subtle and barely detectable.

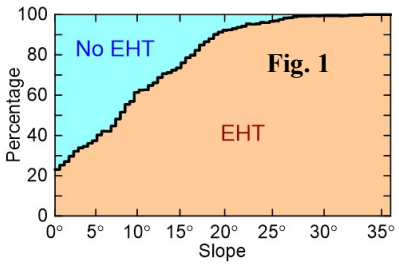

Fig. 1

Topography: Since the visual appearance and apparent anisotropy of EHT depends on the illumination direction, the images are deceptive, and accurate topographic data are needed to understand the nature of EHT relief. At required high resolution, the only available source of topographic information is topography reconstruction from high-resolution images. Two different methods of topography reconstruction are photogrammetry ("shape from stereo") and photoclinometry ("shape from shading"). LROC NAC DTMs [7] from the PDS are generated with photogrammetry. Although those DTMs show some EHT-related topography, their actual resolution and quality is insufficient to study EHT.

Topography from photogrammetry: We studied a photogrammetrically generated DTM of a moderately degraded crater ($D \sim 1.3$ km) at 69.59°S 43.67°E. The DTM was generated with a software complex PHOTOMOD 7.2 [8], which seemingly better deals with small-scale topographic features and produces less resolution-scale noise in comparison to SOCET SET used for PDS DTMs. Another advantage is that our DTM was created from two stereo pairs taken at different illumination directions, which partly eliminates illumination-related bias and reduces effects of source image noise. All 4 source images have high quality and sampling better than 1 m per pixel. The DTM was sampled at 0.5 m/pix to use all potentially available stereo information; its actual resolution is a few meters. Visual inspection showed that this DTM resolves EHT topography much better than "NAC_DTM_BOGSLWSKY1" from the PDS for the same site. At each DTM pixel, we calculated local topographic gradient vector at 4 m baseline, regional gradient by smoothing the DTM with the median filter with a circular window 400 m in diameter, and components of the local gradient in the regional uphill and traverse directions. The scatter diagram (aka 2D histogram) of these two components of the local gradient is shown in **Fig. 2**. It is seen that <u>EHT topography has almost no uphill-faced slopes</u>.

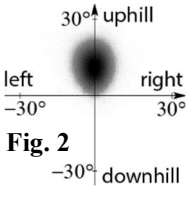

Fig. 2

Topography from photoclinometry: Photoclinometry [e.g., 9] has advantages in comparison to photogrammetry: (1) it potentially produces DTMs of more uniform

quality because it does not depend on availability of small surface details for matching; (2) actual resolution of photoclinometry is higher and potentially can reach the resolution of the source images; (3) if photoclinometric processing uses several source images with sufficiently different illumination directions, the illumination-related biases are weaker. However, photoclinometry is not sensitive enough to gentle regional slopes and its vertical precision depends on knowledge of the photometric function of the surface, which is never perfect. We used "improved photoclinometry" [10, 11], a version of photoclinometric processing yielding topography of the highest probability in the frame of Bayesian inference. We generated DTMs for a few highland sites (~4×4 km) with well-developed EHT from a set of three images with near-optimal illumination directions. Visual inspection showed that the obtained DTMs resolve EHT topography much better than "NAC_DTM_SLIPHER1" from the PDS for the same sites. To focus on topographic details of EHT itself we removed long-baseline topography applying the linear high-pass filter with a circular window ~400 m in diameter. Then we calculated local gradient vectors at 3 m baseline, and expanded them into regional uphill and traverse components for several areas with an approximately constant regional slope. **Fig. 3** shows scatter diagram of these components; the scatter cloud centroid is at the diagram origin due to high-pass filtering. The cloud has a sharp cut-off in the downhill direction (likely due to the absence of slopes facing uphill) and an extended tail in the uphill direction (steep slopes facing downhill). Thus, EHT tends to produce steep downhill-facing slopes (with respect to regional topography).

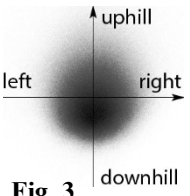

Fig. 3

Scale-dependence: To study scale dependence of EHT roughness we generated a hierarchy of band-pass-filtered topography from the DTMs. Each hierarchy member was obtained by smoothing topography with a median filter with a circular window followed by detrending with a median filter with twice larger window. The use of the median (rather than linear) filters significantly reduces the harmful effects of superposed craters etc. [12]. We manually masked all major irregularities of background topography and small craters; then we calculated the RMS elevation for each hierarchy member as a measure of roughness at a given scale. **Fig. 4** shows RMS elevation as a function of the effective baseline (calculated as a geometric mean of the smoothing and detrending window diameters) in log-log scale for the photogrammetric DTM (blue circles) and one of the photoclinometric DTMs (brown triangles). For the latter, the vertical scale of topography might be biased due to inaccuracy in the photometric function, therefore, vertical position of the brown line in Fig. 3 could be biased; this bias does not affect the slope of the

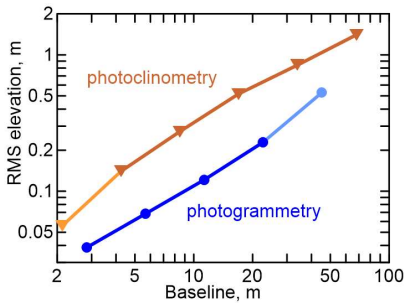

curve. The longest baseline on the blue curve is affected by the crater topography. The shortest baseline of the brown curve is close to the source image resolution and could be biased. With these data points excluded, the curves are remarkably linear, indicating a power-law scale-dependence of roughness with similar exponents (0.85 and 0.83). Moreover, the minor shallowing of the brown curve at longer baselines may be caused, at least partly, by poor sensitivity of the photoclinometric technique to long-baseline topography. Thus, the EHT topography has no any characteristic spatial scale. This is consistent with visual inspection of high-pass-filtered topography revealing no characteristic relief forms.

Constraints on formation mechanism: The fact that the short-baseline slope anisotropy is symmetric with respect to the regional downhill direction confirms the role of slopes in EHT formation. This, taken together with the absence of a distinctive onset slope and the absence of a characteristic spatial scale indicates that the EHT formation is not a growing linear instability of any kind. The absence of a characteristic spatial scale also excludes the role of regolith/substrate interface in EHT formation, EHT formation process operates at the surface and/or in the shallow regolith layers. The absence of uphill-facing short-baseline slopes exclude rotational landslides and other mechanisms that would produce such slopes. It is consistent with subtleness of EHT on very gentle slopes.

Conclusions and future studies: The EHT formation mechanism remains unknown, however we obtained strong constraints on it. Future observations of photometric properties may reveal a role of regolith sorting in EHT formation. Morphological observations of degradation of superposed small craters etc. may give a clue about specific formation mechanism.

References: [1] Plescia & Robinson (2010) EPSC 2010, #731. [2] Antonenko (2012) LPSC 43, #2581. [3] Xiao et al. (2013) EPSL 376, 1. [4] Kreslavsky et al. (2021), LPSC 52, #1826. [5] Soderblom (1970) JGR 75, 2655. [6] Fassett & Thompson (2014) JGR 119, 2255. [7] Henriksen et al. (2017) Icarus, 283, 122. [8] https://en.racurs.ru/about/ [9] Davis & Soderblom (1984) JGR 89, 9449. [10] Parusimov & Kornienko (1973), Astrometry and Astrophysics, 19, 20. [11] Bondarenko et al. (2018) LPSC 49, #2459. [12] Kreslavsky et al. (2017) Icarus 283, 138.